Generation of extremely high angle Bessel beams

Valeria V. Belloni,* **Luc Froehly, Cyril Billet, Luca Furfaro, and Francois Courvoisier****

[1] *FEMTO-ST institute, Université de Franche-Comté, CNRS,*
15B avenue des Montboucons, 25030 Besançon, cedex, France.
*valeria.belloni@femto-st.fr; ** francois.courvoisier@femto-st.fr

Abstract: We present a setup to generate tightly focused Bessel beams, composed of a half-ball lens coupled with a relay lens. The system is simple and compact in comparison with conventional imaging of axicons based on microscope objectives. We experimentally demonstrate the generation of a Bessel beam with 42 degrees cone angle at 980 nm in air with a typical beam length of 500 µm and a central core radius of about 550 nm. We studied numerically the effects of misalignment of the different optical elements and the range of tilt and shift that are acceptable to obtain a regular Bessel beam.

1. Introduction

The Bessel beam finds application in numerous fields thanks to its peculiar properties. It was first recognized as a propagation-invariant solution to the Helmholtz equation in 1987 by Durnin *et al.* [1]. The beam is generated by the interference of plane waves in a conical geometry, with an angle of interference called *cone angle* [2]. Its transverse profile is invariant during propagation and is featured by an intense central core surrounded by weaker concentric rings. The central core of the beam can reach a very high aspect ratio, since the radius of the core and its length depend on two independent parameters, in contrast with the Gaussian beam where the waist and Rayleigh range cannot be independently controlled. The large depth of field of the Bessel beam and the high contrast between the central core and the rings fit well the needs of the processing of transparent material, like drilling [3–5] and cutting [6]. Moreover, high-aspect ratio central core allows a long working range that is useful when the position focus-sample is critical, as in the process of curved surfaces [7] and in the welding of different materials [8]. Another advantage of the Bessel beam is the self-reconstruction property that allows the regeneration of the beam after an obstacle. This last feature is particularly beneficial for microscopy techniques, one example is the light sheet microscopy [9, 10]. It can be used also to study non-linear processes [11], in optical trapping [12], in the generation of warm dense matter over a long distance [13], or in creating long plasma tracks to guide discharges [14].

Some applications, such as material processing and particle acceleration, require a very high intensity in the central core. This can be reached at constant input pulse energy by increasing the focusing angle of the Bessel beam. It has been shown theoretically and experimentally that a higher angle Bessel beam allows obtaining channels in transparent materials thanks to the reduction of the screening effect of the plasma [15]. In fact, to cut or drill transparent materials, the Bessel beams used have angles in the range between 17° and 26° in air, that lead due to refraction to angles between 10° and 16° in a medium with refractive index ~1.5 [3, 16]. A higher angle Bessel beam leads to a smaller central core radius as the FWHM of the central peak follows: $d_{\mathrm{FWHM}} = 0.36\frac{\lambda}{\sin\theta}$.

The theoretical studies on the generation of large angle Bessel beam provided interesting setup configurations. For example, the use of a 90° apex-angle concave conical mirror with a radially polarized beam allows to generate a really high aspect-ratio Bessel beam with a length of

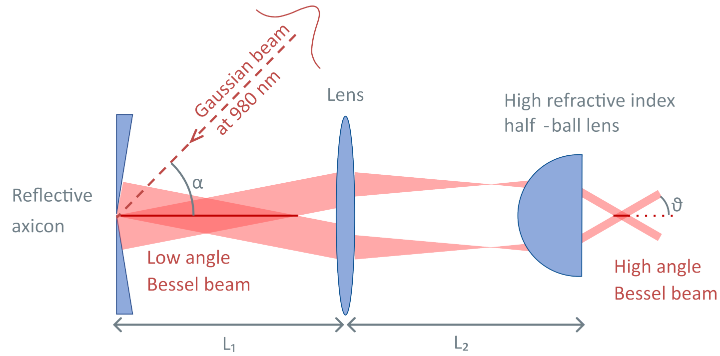

Fig. 1. Schematic of the setup for the generation of high angle Bessel beam. The Gaussian beam at 980 nm generates a low angle Bessel beam thanks to a reflective axicon of 2 degrees, the Bessel beam is then demagnified with a telescopic system composed by a lens of 35 mm focal length and a half-ball lens. The half-ball lens has a diameter of 8 mm and it is made of S-LAH79 (refractive index: 1.97 at 980 nm).

50000λ and a central core dimension of 0.36λ [17]. However, the use of a reflective axicon with very high angle is incompatible with the insertion of a sample. Another theoretical setup, that overcomes this problem, uses a combination of a binary phase plate and a doublet including a high NA 0.95 lens [18]. The computed Bessel beam has a central core size (FWHM) of 0.39λ (cone angle of $67.6°$).

The standard technique to generate a high-angle Bessel beam uses a telescopic system: a primary low angle Bessel beam, created using an axicon, a spatial light modulator or a fluidic axicon [19], is imaged using a high magnification 2f-2f telescope. To reach high magnifications, the second lens is a microscope objective [20]. However, not only the overall setup is very long because of the length of the telescope, but also the intensity distribution impinging on the second optical element, the microscope objective, is in the shape of a thin ring. The high intensities used for laser materials processing can easily lead to damage of a costly optical element. Another technique, that takes advantage of the combination of three axicons, allows to reach energies up to the Joule level, but it is limited to a cone angle of 26 degrees (FWHM 0.82λ) by the manufacturability of high base angle axicons [16, 21].

Here, we propose a compact experimental setup that overcomes the limitations of the previous techniques using a half-ball lens. The half-ball lens helps to generate very high angle Bessel beams, up to $42°$, thanks to the high refractive index and the high curvature. Simultaneously, the absence of glue in the half-ball lens leads to a higher damage threshold when compared to a conventional microscope objective. Since strong focusing is conventionally associated with delicate alignment, we analyze the different positioning constraints on the system.

2. Experimental setup

We generate the high angle Bessel beam with the setup shown in Fig. 1, using as a laser source a laser diode at 980 nm. The Gaussian beam has a waist of ≈ 3 mm (diameter at $1/e^2$) and impinges on a reflective axicon of 2 degrees base angle (Canunda axicon AX-2-25-S) at an incidence angle of $\alpha = 30$ degrees. This allows generating a primary Bessel beam with a cone angle of 4 degrees. Then, the beam cone angle is increased using a telescopic system composed of a lens (focal length 35 mm) and a 8 mm diameter half-ball lens. The material of the half-ball lens is S-LAH79 which is a high refractive index dielectric, with a value of 1.97 at the used wavelength. The shaped beam illuminates only a restricted area of the half-ball lens, shaped as a thin ring of thickness 200 µm. This is in agreement with the commonly accepted rule of thumb

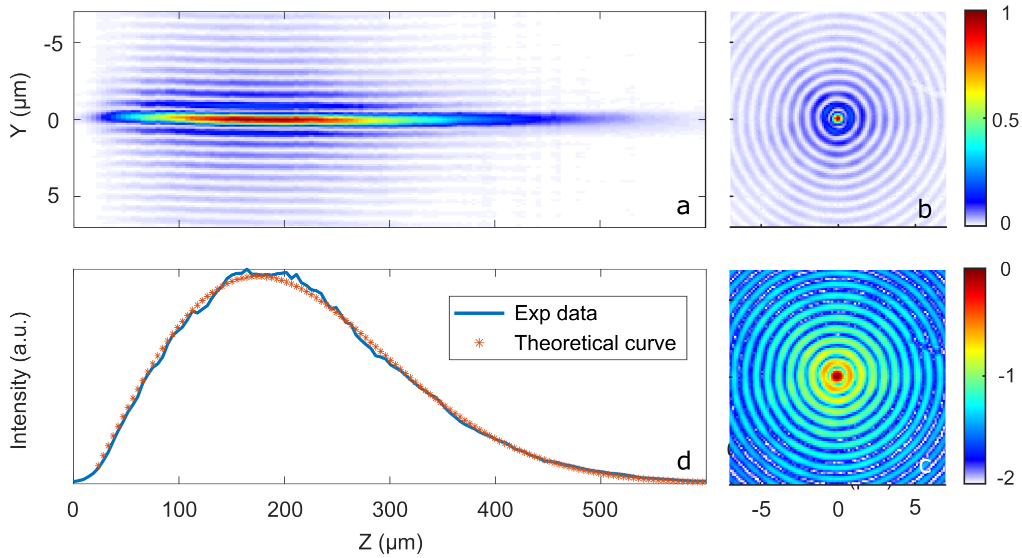

Fig. 2. Intensity distribution of the Bessel beam, with wavelength 980 nm, featured by a central core of 523 nm (FWHM), corresponding to an angle of 43 degrees, and a length of about 500 µm (FWHM 250 µm). (a) Section of the scan; (b) Cross-cut in linear scale at z = 160 µm; (c) Cross-cut in logarithmic scale z = 160 µm. (d) Experimental and theoretical data of the evolution of the central core intensity;

of using lenses with beam diameters of only 1/10 of the focal length to avoid aberrations. Here, the limit is therefore ~500 µm. For this reason, the high curvature does not introduce measurable spherical aberrations and all optical rays are identically refracted.

The ideal distance between the axicon and the relay lens (L_1) is 90 mm and the one between the relay lens and the half-ball lens (L_2) is 30 mm. We will see in the last section that these distances are relatively flexible to produce a Bessel beam.

We image the beam using an imaging system composed of a microscope and relay lens that leads to a magnification of 110. The full imaging system is placed on a motorized translation stage, which allows us to scan the beam along the propagation direction.

3. Experimental results

We show our experimental results in Fig. 2. In Fig. 2(a), we plot the longitudinal cross-section of the intensity distribution as a function of propagation distance, where we see the parallelism of the lobes and that the Bessel beam length is of about 500 µm equal to 510λ (FWHM 250 µm or 255λ). Fig. 2(b) shows the transverse cross-section at a distance corresponding to the peak of the longitudinal distribution (z = 160 µm). The same distribution is shown with a logarithmic scale in Fig. 2(c), which features the high degree of symmetry and quality of the Bessel beam produced. The dimension of the central core changes slightly along the beam, which means that the angle of the Bessel beam is not perfectly constant. In our case, the first part of the beam is featured by a central core of 523 nm (FWHM), *i.e.*, 0.53λ, which corresponds to an extremely high angle of $\theta = 42$ degrees (measured at z = 90 µm), and the end of the beam has a central core of 554 nm (FWHM) *i.e.*, 0.56λ, which corresponds to an angle of $\theta = 40$ degrees (measured at z = 325 µm). We obtained the dimension of the central core by fitting its intensity with a zeroth-order Bessel function with an error of 1 degree on the angle estimations.

In Fig. 2(d), we compare the evolution of the on-axis intensity distribution to the one of an ideal Bessel-Gauss beam, which follows [3, 22]:

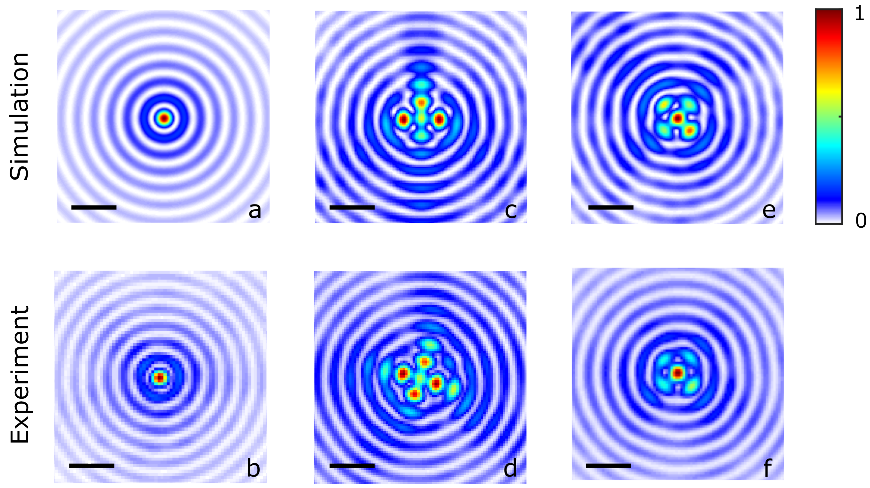

Fig. 3. Comparison between the simulations obtained with Zemax OpticStudio™ and the experimental results. We compared the undistorted Bessel beam (Fig. a simulated and Fig. b experimental), an axicon tilt of 0.14° (Fig. c simulated and Fig. d experimental) and the effect of 50 µm shift of the half-ball lens (Fig. e simulated and Fig. f experimental). Scale bars are 2 µm.

$$I(z) = \frac{8\pi P_0 z}{\lambda} \frac{\sin^2\theta}{w^2} \exp\left[-2\left(\frac{z\sin\theta}{w}\right)^2\right]$$

where P_0 and w are respectively peak power and the waist of the input Gaussian beam, θ is the cone angle of the Bessel beam. We can see that the experimental data is in excellent agreement with the theoretical one.

4. Analysis of the setup

We have simulated our setup from the reflective axicon to the high angle Bessel beam using the software Zemax OpticStudio™. This analysis aimed to investigate how critical is the positioning of each element and the effects on the final beam shape. For the simulations, we have modelled the axicon using an ideal off-axis reflective axicon with a phase profile given by $\Phi(x, y) = (2\pi/\lambda)\ \tan\beta\sqrt{\cos^2(\alpha)\, x^2 + y^2}$ [20]. We used the optical design of the relay lens provided by the supplier and we modeled the half-ball lens with the high refractive index 1.97. The system was optimized to produce the desired cone angle and the parallelism of the rays of the Bessel beam, which means a constant angle for the entire beam. We used the Zemax Point Spread Function, based on Huygens wavelet principle, to compute the final intensity distribution in the Bessel zone. We provide below the maximum deviations in tilt or shift from the ideal position before which the high angle Bessel beam starts to lose its characteristic cylindrical symmetry, particularly in the first lobe (see Fig. 3). We compare in Fig. 3, the simulated and the experimental results. For comparison, the undistorted beam is shown in (a) for the simulation part and in (b) for the experimental one.

The axicon has been manufactured to be operated under an incidence angle of $\alpha = 30°$. Our simulations show that, to maintain an acceptable symmetry of the intensity distribution, the maximum deviation from the ideal angle is about 0.08°: the increase in the deviation leads to a change in the shape of the first ring into four lobes as we can see in Fig. 3 (c) and (d) where the tilt applied to the axicon is 0.14° for the simulated and the experimental results, respectively.

This distortion progressively grows from the end of the beam, as can be expected from an axicon illuminated under oblique incidence [23].

The distance between the axicon and the relay lens (L_1) is not critical. It can be varied over a range of about 40 mm around the ideal position of 90 mm (±22%), while the only impact on the Bessel beam is to slightly change its cone angle by 1° to 2°. In this case, the cone angle is still homogeneous along the beam. The distance between the relay lens and the half-ball lens (L_2) is also not critical within a smaller range of 1 mm to 2 mm, but a deviation from the ideal position of 1 mm induces a variation of the angle between the beginning and the end of the Bessel beam of 1° to 2° over the 200 µm length of the Bessel beam. The small error in the longitudinal positioning of the two lenses introduces a quadratic term. The consequence is that the wavevectors undergo slightly different refraction and are not perfectly parallels. The result is a varying angle along the propagation direction. This case corresponds to the "accelerating" or "decelerating" Bessel beams first reported in Ref. [24]. The half-ball lens allows having a deviation from the ideal position of 1° for the tilt. In contrast, the centering of the half-ball lens is relatively critical as it requires a precision of typically 30 µm. In Fig. 3 (e), we show the result of the beam for a de-centering of 50 µm and the corresponding experimental result (f). In this case, the first side lobe gets split into four parts. We finally note that our simulation results are in good agreement with our experimental observations.

In addition to the positioning constraints, we studied the flexibility of the system regarding different wavelengths. We could obtain a high cone angle Bessel beam for a range of wavelength that varies from 0.5 µm to 2 µm. Due to the chromatic dispersion, the positioning of the different lenses had to be adjusted for each case to obtain a regular Bessel beam.

5. Conclusion

We have experimentally demonstrated a novel design for Bessel beam generation with a high focusing angle using a simple optical setup. We were able to experimentally reach an extremely high angle of 42° (equivalent numerical aperture of NA 0.67). This was made possible by the use a half-ball lens with a high refractive index. This configuration brings different advantages: the setup is at least 5 times more compact in comparison with a standard demagnification system and more cost-effective. Moreover, the usable wavelength range varies from the VIS to the near IR. Importantly, the damage threshold of the half-ball lens is much higher compared to the one of a microscope objective, particularly because of the absence of glue.

In addition, we have analyzed, using numerical simulations the constraints on the positioning of the optical elements. Our analysis reveals that only two parameters are relatively critical: the incidence angle on the reflective axicon should be accurate within 0.08° and the centering of the half-ball within 30 µm. Finally, our approach is also compatible with spatial filtering [25], as well as polarization [18] or transversal shaping techniques [26, 27]. We believe that this simple and compact setup can provide new perspectives for the study of laser-matter interaction with Bessel beams in unconventional configurations.

Funding. This project is an initiative of the Photonics Public Private Partnership and has received funding from the European Union's Horizon 2020 research and innovation programme under grant agreement No 825246 kW-flexiburst. This research has also received funding from H2020 European Research Council (ERC) under grant agreement 682032-PULSAR and Agence Nationale de la Recherche (EQUIPEX+ SMARTLIGHT platform ANR-21-ESRE-0040), and the EIPHI Graduate School (ANR-17-EURE-0002).

Acknowledgments. Technical assistance by E. Dordor is gratefully acknowledged.

Disclosures. The authors declare no conflicts of interest.

Data Availability Statement. Data underlying the results presented in this paper are not publicly available at this time but may be obtained from the authors upon reasonable request.

References

1. J. Durnin, J. Miceli, J. J., and J. H. Eberly, “Diffraction-free beams,” Phys. Rev. Lett. **58**, 1499–1501 (1987).
2. D. McGloin and K. Dholakia, “Bessel beams: Diffraction in a new light,” Contemp. Phys. **46**, 15–28 (2005).
3. M. Bhuyan, F. Courvoisier, P. Lacourt, M. Jacquot, R. Salut, L. Furfaro, and J. Dudley, “High aspect ratio nanochannel machining using single shot femtosecond Bessel beams,” Appl. Phys. Lett. **97**, 081102–081102 (2010).
4. M. Duocastella and C. Arnold, “Bessel and annular beams for materials processing,” Laser & Photonics Rev. **6**, 607–621 (2012).
5. L. Rapp, R. Meyer, R. Giust, L. Furfaro, M. Jacquot, P.-A. Lacourt, J. Dudley, and F. Courvoisier, “High aspect ratio micro-explosions in the bulk of sapphire generated by femtosecond Bessel beams,” Sci. Reports **6**, 34286 (2016).
6. R. Meyer, L. Froehly, R. Giust, J. Del Hoyo, L. Furfaro, C. Billet, and F. Courvoisier, “Extremely high-aspect-ratio ultrafast Bessel beam generation and stealth dicing of multi-millimeter thick glass,” Appl. Phys. Lett. **114**, 201105 (2019).
7. X. Li, Z. Xu, L. Jiang, Y. Shi, A. Wang, L. Huang, and Q. Wei, “Creating a three-dimensional surface with antireflective properties by using femtosecond-laser Bessel-beam-assisted thermal oxidation,” Opt. Lett. **45** (2020).
8. G. Zhang, R. Stoian, W. Zhao, and G. Cheng, “Femtosecond laser bessel beam welding of transparent to non-transparent materials with large focal-position tolerant zone,” Opt. Express **26**, 917 (2018).
9. L. Gao, L. Shao, B. Chen, and E. Betzig, “3D live fluorescence imaging of cellular dynamics using Bessel beam plane illumination microscopy,” Nat. protocols **9**, 1083–101 (2014).
10. S. Takanezawa, T. Saitou, and T. Imamura, “Wide field light-sheet microscopy with lens-axicon controlled two-photon Bessel beam illumination,” Nat. Commun. **12**, 2979 (2021).
11. P. Polesana, M. Franco, A. Couairon, D. Faccio, and P. Trapani, “Filamentation in Kerr media from pulsed Bessel beams,” Phys. Rev. A - PHYS REV A **77** (2008).
12. T. Čižmár, V. Garces, K. Dholakia, and P. Zemanek, “Optical trapping in counter-propagating Bessel beams,” Proc. SPIE - The Int. Soc. for Opt. Eng. **5514** (2004).
13. J. del Hoyo, R. Meyer, L. Furfaro, and F. Courvoisier, “Nanoscale confinement of energy deposition in glass by double ultrafast Bessel pulses,” Nanophotonics **10**, 1089–1097 (2021).
14. M. Clerici, Y. Hu, P. Lassonde, C. Milian, A. Couairon, D. N. Christodoulides, Z. Chen, L. Razzari, F. Vidal, F. Legare, D. Faccio, and R. Morandotti, “Laser-assisted guiding of electric discharges around objects,” Sci. Adv. **1**, e1400111–e1400111 (2015).
15. R. Beuton, B. Chimier, P. Quinoman, P. González de Alaiza Martínez, R. Nuter, and G. Duchateau, “Numerical studies of dielectric material modifications by a femtosecond Bessel–Gauss laser beam,” Appl. Phys. A **127** (2021).
16. R. Meyer, L. Froehly, R. Giust, J. Hoyo, L. Furfaro, C. Billet, and F. Courvoisier, “Extremely high-aspect-ratio ultrafast Bessel beam generation and stealth dicing of multi-millimeter thick glass,” Appl. Phys. Lett. **114**, 201105 (2019).
17. M. Zhu, Q. Cao, and H. Gao, “Creation of a $50,000\lambda$ long needle-like field with 0.36λ width,” J. Opt. Soc. Am. A **31**, 500–504 (2014).
18. R. K.B, Z. Jaroszewicz, and P. Anbarasan, “Improvement of lens axicon’s performance for longitudinally polarized beam generation by adding a dedicated phase transmittance,” Opt. express **18**, 26799–805 (2010).
19. G. Milne, G. Jeffries, and D. Chiu, “Tunable generation of bessel beams with a fluidic axicon,” Appl. Phys. Lett. **92**, 261101 – 261101 (2008).
20. P. Boucher, J. Del Hoyo, C. Billet, O. Pinel, G. Labroille, and F. Courvoisier, “Generation of high conical angle Bessel-Gauss beams with reflective axicons,” Appl. Opt. **57**, 6725–6728 (2018).
21. K. Bergner, M. Müller, R. Klas, J. Limpert, S. Nolte, and A. Tünnerman, “Scaling ultrashort laser pulse induced glass modifications for cleaving applications,” Appl. Opt. **57**, 5941–5947 (2018).
22. V. Jarutis, R. Paškauskas, and A. Stabinis, “Focusing of Laguerre-Gaussian beams by axicon,” Opt. Commun. **184**, 105–112 (2000).
23. A. Burvall, K. Kolacz, A. V. Goncharov, Z. Jaroszewicz, and C. Dainty, “Lens axicons in oblique illumination,” Appl. Opt. **46**, 312–318 (2007).
24. M. Clerici, D. Faccio, A. Lotti, E. Rubino, O. Jedrkiewicz, J. Biegert, and P. D. Trapani, “Finite-energy, accelerating Bessel pulses,” Opt. Express **16**, 19807 (2008).
25. O. Brzobohatý, T. Čižmár, and P. Zemanek, “High quality quasi-bessel beam generated by round-tip axicon,” Opt. express **16**, 12688–700 (2008).
26. R. Meyer, M. Jacquot, R. Giust, J. Safioui, L. Rapp, L. Furfaro, P.-A. Lacourt, J. M. Dudley, and F. Courvoisier, “Single-shot ultrafast laser processing of high-aspect-ratio nanochannels using elliptical bessel beams,” Opt. Lett. **42**, 4307–4310 (2017).
27. J. Dudutis, M. Mackevičiūtė, J. Pipiras, R. Stonys, V. Stankevič, G. Raciukaitis, and P. Gecys, “Transversal and axial modulation of axicon-generated bessel beams using amplitude and phase masks for glass processing applications,” Opt. Express **30**, 1860–1874 (2021).